Time evolution of mining-related residual subsidence monitored over a 24-year period using InSAR in southern Alsace, France

Guillaume Modeste, Cécile Doubre, Frédéric Masson

International Journal of Applied Earth Observations and Geoinformation 102 (2021) 102392

Contents lists available at ScienceDirect

International Journal of Applied Earth Observations and Geoinformation

journal homepage: www.elsevier.com/locate/jag

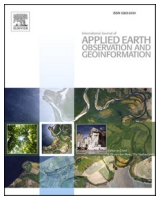

Time evolution of mining-related residual subsidence monitored over a 24-year period using InSAR in southern Alsace, France

Guillaume Modeste *, Cécile Doubre, Frédéric Masson

Institut de Physique du Globe de Strasbourg (IPGS), 5 rue René Descartes, 67084 Strasbourg, France

ARTICLE INFO

Keywords:
Persistent scatterer interferometry
Residual subsidence
Salt mine
Longwall mining
Upper Rhine Graben

ABSTRACT

From 1910 to 2002, the Mines Domaniales de Potasse d'Alsace (MDPA) exploited two potash layers, located at depths greater than 400 m in the southern Upper Rhine Graben. This mining activity has caused surface subsidence, investigated here using SAR interferometry (InSAR) and Persistent Scatterer Interferometry (PSI) approach is used to follow mining induced surface displacements over the Alsatian potassic basin. The SAR images acquired by three distinct satellites (ERS, ENVISAT, Sentinel-1) over the last 24 years cover both mining and post-mining periods. Until 1996/1997, InSAR results do not fit the high vertical displacement deduced from levelling campaigns due to unwrapping errors and are therefore not reliable to quantify the mining subsidence. From 1996/1997, InSAR results and levelling measurements become consistent, allowing us to study the subsidence following the activity of the mine. The surface subsidence decreases quickly after the end of mining operations, with current subsidence estimated below 5 mm/yr in 2018. The InSAR results obtained for the post-mining period show a correlation between residual subsidence amplitude and the mined thickness. Taking together the InSAR and levelling measurements for the whole 24 years period, the combined time series are approximated by a sum of two exponential terms, which reveals the role of the goaf compaction at depth. The study shows that SAR interferometry is well suited for monitoring small amplitude mining-induced subsidence over the residual phase, helping to better mitigate the related risk in these regions.

1. Introduction

Ground subsidence could be the first visible consequence of mining activity, with displacements potentially reaching several decimetres and causing damage to man-made infrastructures. In north-eastern France, the 92 years of activity by the Mines Domaniales de Potasse d'Alsace (MDPA) represent an interesting example of mining-induced subsidence issues. Large surface displacements have generally been detected during the period of mining and are mainly dominated by subsidence traditionally surveyed using levelling (Chrzanowski et al., 1997) techniques with repeated measurement campaigns at specific instrumented points reaching an accuracy of a few millimetres.

A large range of models has been developed and proposed to anticipate the mining subsidence in terms of displacement amplitude, spatial distribution and time evolution, and eventually to mitigate the damages (Kratzsch, 1983; Whittaker and Reddish, 1989). From the observation conducted at several mining sites, three distinct phases of the surface subsidence are identified for a point located at surface over the area of exploitation (Al Heib et al., 2005; Fig. 1) and are represented by the qualitative model in Fig. 1. The subsidence rate increases during the initial phase, then becomes linear over the mining phase and lastly, decreases through the residual phase. The duration of the mining subsidence ranges from a few months to several decades (Yao and Reddish, 1994). The two first phases are considered to be active subsidence, contrasting with the third known as delayed subsidence. The qualitative model presented in Fig. 1 and the relative amount of displacement for the three phases are based on surface observations from levelling campaigns over the MDPA concessions (internal communication). Many parameters control the amount of displacements occurring over each phase (Kratzsch, 1983; Whittaker and Reddish, 1989) and reliable estimates of the surface displacements over a long time period allow a better estimates of their respective impacts.

The development of new techniques, in particular remote sensing, have revolutionized the quantification of surface displacements caused by natural (Massonnet and Feigl, 1998) or anthropic (Amelung et al., 1999) sources. Interferometric Synthetic Aperture Radar (InSAR) allows the tracking of the displacement field along the Line of Sight (LOS) of the radar for a wide surface area with a resolution of 1–25 m. The accuracy

* Corresponding author.
E-mail addresses: guillaume.modeste@univ-lorraine.fr (G. Modeste), cecile.doubre@unistra.fr (C. Doubre), frederic.masson@unistra.fr (F. Masson).

https://doi.org/10.1016/j.jag.2021.102392
Received 18 December 2020; Received in revised form 31 May 2021; Accepted 6 June 2021

of the displacement is of millimetres to centimetres, depending both on the characteristics and the number of SAR images, and on the persistence of the surface scattering properties. InSAR measurements have been applied for monitoring mining induced subsidence over active mines (Colesanti et al., 2005). Residual mining subsidence has been monitored from 1992 to 2007 in the Nord/Pas-de-Calais (France) coal basin (Guéguen et al., 2009), up to 16 years after the end of mining activity, and from 1995 to 2009 in the Lorraine (France) coal basin (Samsonov et al., 2013).

In this study, we focus on the surface subsidence and its evolution over the period 1995–2018 induced by the extraction of potash ore, which ended in 2002 in the Alsatian potassic basin. A previous InSAR study showed the benefits and limitations of the techniques to detect the mining subsidence during the activity of the mine (1992–1993, Raymond and Rudant, 1997). A combination of space geodetic techniques in the whole Rhine Graben and surroundings revealed significant signals over the mining concessions for the period 1992–2010 (Fuhrmann, 2016). From 1996/1997, our InSAR results show consistency with available levelling measurements and highlight the occurrence of mining subsidence over decades. Surface displacements are shown to be mainly related to the underground activities. This late subsidence is connected to the visco-plastic responses of the overburden and the compaction of caved zones. From these results, the residual subsidence seems to be directly related to the mined thickness.

2. Potash mining in the south of Alsace

2.1. Geological context

At the beginning of the 20th century, with the hydrocarbon exploration in the Rhine Graben two layers of potash separated by 20 m were found over an area of hundreds of square kilometres at a depth of 450 m to 1150 m in the North of Mulhouse (Fig. 2). These potash deposits, unique to the southern part of the Rhine Graben, are quite heterogeneous in terms of both depth and thickness. Their continental or marine origin remains a topic of debate (Cendon et al., 2008). The potash layers belong to a several 100 m thick evaporitic deposit constituted by a variety of marls at the top and three levels of different combinations of marls, anhydrites and rock salt (Table 1). The sylvinite, the main mineral of the potash, is present in the shallow level. Above the potash layers, the Vosges alluviums filled the basin (clays, sands, …).

2.2. History of the exploitation and subsidence monitoring

The drilling characteristics and the industrial interests in potash conducted to the exploitation by the MDPA in 1910. For 92 years, the MDPA had access to more than 200 km^2 of concession and exploited both layers of potash in less than two thirds of this area, divided into the eastern and the western sectors due to a flexure in the deposit layers (Fig. 2). Various methods of ore extraction were used over the years, such as room and pillars or longwall, and were mainly coupled with caving. The use of caving concerned about 90% of the total mined panels. Since 1980, the ore was only extracted by longwall mining.

To monitor the subsidence related to the mining activity, levelling campaigns have been conducted regularly from 1990 to 2002, with a mean repetition time of one month. These measurements were carried out in the vicinity of the ongoing extraction at depth.

In this study, our analysis concerns the panels in the vicinity of these levelling points. The depth of these panels is similar, i.e. 850 m at Raedersheim, 900 m at Pulversheim and 1000 m at Pulversheim. The mined thickness is lower at Raedersheim (3.05 m) than Bollwiller (3.90 m) and Pulversheim (4.00 m).

3. Methods and data

3.1. Persistent scatterer and small baseline processing

The radar interferometry (InSAR) allows the measurement of the ground displacement using the phase variation of two co-registered SAR images acquired over the same region at two distinct times. InSAR method is currently used in Earth Sciences to quantify the surface displacement field for a better understanding of natural processes (eg., Massonnet and Feigl, 1998), but also for monitoring anthropic induced ground deformation (Oppliger et al., 2006). The growing archives of available SAR images allow the use of this technique for tracking the surface displacement field over a long period (Declercq et al., 2017).

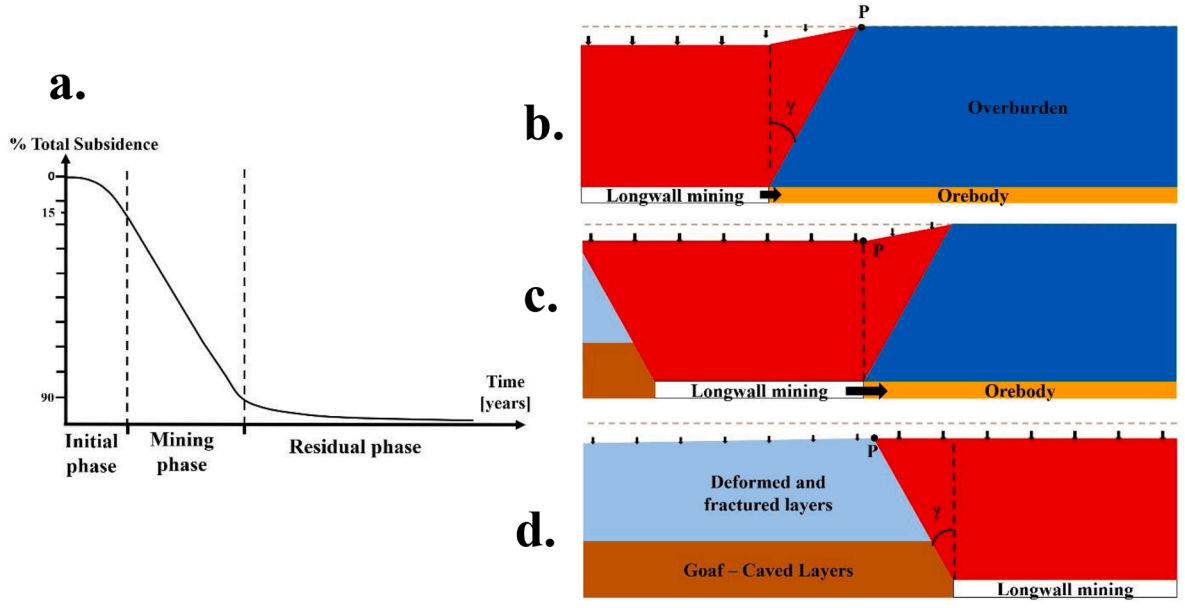

Fig. 1. Mining subsidence through time. (a) Time evolution of mining-induced subsidence. (b–d) Schematic profile of the ongoing exploitation at depth showing the time evolution of the influence area (red area). The initial phase (b) starts when the point enters in the influence area, which depends on γ, the angle of draw. The mining phase (c) begins when the point is above the ongoing mining at depth. Last, the residual phase (d) starts when the point leaves the influence area. (For interpretation of the references to color in this figure legend, the reader is referred to the web version of this article.)

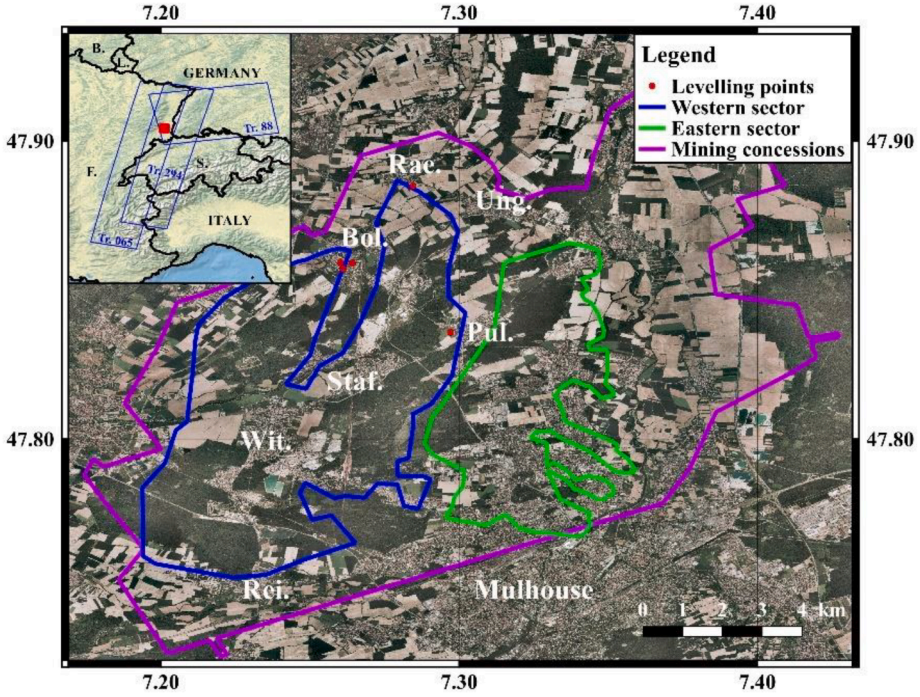

Fig. 2. Map of the Alsatian potassic basin. The background is the IGN orthophotography (2002). Bol.: Bollwiller, Pul.: Pulversheim, Rae.: Raedersheim, Rei.: Reiningue, Staf.: Staffelfelden, Wit.: Wittelsheim, Ung.: Ungersheim. Inset: Location of the MDPA (red square) at the regional scale. Blue rectangles represent the coverage of each track of SAR images. B.: Belgium, L.: Luxembourg, F.: France, S.: Switzerland. (For interpretation of the references to color in this figure legend, the reader is referred to the web version of this article.)

Table 1
Synthetic geological log of the Alsatian potassic basin.

Epoch	Period	Geology	Range thickness
Pliocene	Quaternary	Vosges alluvium, clays	5–250 m
Oligocene	Chattian	Carbonate, gypsum, marls	Up to 445 m
	Rupelian	Marls, shales	Up to 420 m
		Marls with gypsum or anhydrite	
		Marls with rock salt and anhydrite	Up to 580 m
		Potash layers	
Eocene	Priabonian	Fossiliferous zone (marls)	Up to 300 m
		Marls with rock salt and anhydrite	
		Marls with rock salt and anhydrite	Up to 860 m
		Green marls	
Jurassic	–	Basal clay	0–100 m
		Lake limestone	
		Oolithic marls	–

adapted from Blanc-Valleron, 1991

Because the region under study is covered by agricultural fields and forests, for ~70% of the mining concession surface, volumetric and temporal decorrelations affect the InSAR results. Thus, we used the Persistent Scatterer (PS) method implemented in the Stanford Method for Persistent Scatterer (Hooper et al., 2012) (StaMPS). This method takes advantage of the presence of dominant reflectors, such as a roof or a wall or any other human-made structures which persist over time (Hooper et al., 2012). For the ERS and ENVISAT images, all the interferograms are calculated with respect to the same reference image (master). A similar processing chain has been developed on Sentinel Application Platform (SNAP) to process Sentinel-1 data specifically (Foumelis et al., 2018). For each dataset, a first selection is made with the amplitude dispersion of each pixel, in order to keep those that return stable signal over time. This step aims to cancel out pixels whose surface area varies over time, such in fields or forests. A second selection is made according to the average noise level in the phase of each pixel (Hooper et al., 2007). The unwrapping step is made for the selected pixels, in spatial and temporal dimensions, in order to reconstitute the time evolution of displacement (Hooper and Zebker, 2007).

To improve the quality of the results, the Small Baseline (SB) method has been implemented on StaMPS and combined with the PS method (Berardino et al., 2002; Shanker et al., 2011) for ERS and ENVISAT data. The SB method consists in computing interferograms with small perpendicular and temporal baselines to reduce both spatial and temporal decorrelations. The orbital effect is modelled from orbital data and removed from the signal. Taking into account the small size of our studied area characterized by a flat topography, the atmospheric signal, mainly due to the vapor-water content in the troposphere with the use of C-band SAR images, can be considered as homogeneous within each interferogram (Hanssen, 2010). Also, the use of a reference zone allows us to assume the atmospheric errors to be negligible over time. In addition, the topographic errors, which would be revealed by a correlation between the phase values and the perpendicular baselines, are very small. The time series of the LOS displacement are retrieved to estimate the incremental displacement at each time of the image acquisitions (Hooper et al., 2012), by averaging the incremental displacements of all the pixels located within a ≃100 m-radius circle. The standard deviation of these incremental displacements is used to evaluate the displacement uncertainty at each date. The mean LOS velocity map is computed for the whole duration of each archive by estimating the linear regression of the displacements over time with a least square method. Using a bootstrap method, the dispersion of the regression results is used to estimate the standard deviation of the computed velocity, which is taken as the uncertainty on the mean velocity.

3.2. SAR archives

We analyse the large archives of the C-band SAR images independently from three satellites of the European Space Agency (ESA). The ERS, ENVISAT and Sentinel-1 data cover the periods from 1995 to 2000, from 2004 to 2010, from 2015 to 2018, respectively (Table 2). The minimum repetition time of acquisition is 35 days for the ERS and ENVISAT satellite, and 12 days from November 2014 to September 2016 and 6 days from October 2016 to December 2018 for the Sentinel-1 satellites.

In order to estimate the topographic contribution, we use the digital elevation model from the Shuttle Radar Topography Mission (SRTM, Farr and Kobrick, 2000) with a resolution of 30 m.

In addition to the SAR archives, levelling measurements are available

Table 2
Characteristics of the SAR image archives used in this study.

Satellite	Track number	Path (heading angle)	Number of SAR images	Look/incidence angles (°)	Time period	Associated period of the exploitation
ERS	29	ascending (N-15.2°E)	29	21.5/24.3	04/1995–05/2000	Mining
ERS	65	descending (N-164.8°E)	51	17.8/20.1	09/1995–12/2000	Mining
ERS	294	descending (N-164.8°E)	62	21.2/24	04/1995–12/2000	Mining
ENVISAT	294	descending (N-164.8°E)	42	21.4/24.3	12/2003–10/2010	Post-mining
Sentinel-1	66	descending (N-171.2°E)	145	39.9/43.7	03/2015–12/2018	Post-mining
Sentinel-1	88	ascending (N-9.7°E)	186	36.1/38.9	11/2014–12/2018	Post-mining

at specific points. The available levelling data concern five sites mainly located in the towns above the most recent panels (Fig. 2). The levelling sites of Bollwiller are in the town, while the sites of Pulversheim and Raedersheim are at the border of the towns. The vertical displacements associated with the mining period were estimated using levelling techniques to reach 278 cm over 9 years, with an accuracy of 1 cm.

4. Results

The analysis of the surface velocity fields is constrained at the retained pixels which are located mainly over urbanized areas and human infrastructures (Fig. 3), corresponding approximately to one third of the concession area for each track of the satellites.

4.1. Surface velocity fields

In order to analyse the spatial variation of the surface velocity, we present maps of the mean LOS velocity of the ground over the three periods under study corresponding to the three archives of SAR images (Fig. 4a–c). Surface displacements are detected at every period, including the latest period of Sentinel-1 observations (2015–2018), suggesting the occurrence of surface displacements 13 years after the end of the mine activity. The largest displacement rates for each period are localised over areas of lateral extension smaller than 1 km^2, in villages located above the recent panels such as Bollwiller, Pulversheim and Staffelfelden (Fig. 4a). The amplitude of the surface velocity decreases over time. The LOS velocity amplitudes from ERS and ENVISAT data can be directly compared since the azimuth and incident angles are similar. However, this is not the case for Sentinel-1 data (Table 2). The maximum LOS velocity reaches about ~84 ± 9.5 mm/yr for the ERS period (1995–2000), and drops down ~ 15 ± 1.3 mm/yr for ENVISAT period (2004–2010). If we assume that displacements are mainly vertical, we observe a decrease of about 30% of the maximum vertical velocity between the ENVISAT and the Sentinel-1 periods. The LOS displacement being the component of the real displacement assumed here to be vertical, this latter can be retrieved by the relation $D_v = D_{LOS}/\cos(i)$ with i the angle of incidence at the considered pixels (Table 2).

In the village of Staffelfelden, fast displacements of the ground occur during the ENVISAT (2004–2010) and Sentinel-1 (2015–2018) periods (Fig. 4b-c), with motion reaching a LOS rate over 8 mm/yr away from the satellite.

The Fig. 4 d, e and f show the spatial distribution of the standard deviation of the mean LOS velocity field. High standard deviation values are associated with non-steady state displacements, mostly observed during the first period of observation (ERS, 1995–2000) with values exceeding 9 mm/yr, in Bollwiller and Pulversheim. The amplitude of the standard deviation decreases over the three periods, to become more homogeneous within the area of study. The relatively high standard deviation for the stable areas during the ERS period, between 2 and 3 mm/yr, is mainly due to the lower number of interferograms used in this period with respect to the Envisat period. Regarding the Sentinel-1 period, the large number of images used for the processing together with the very low standard deviation confirms the stationary displacements. The following time series analysis of the LOS displacements

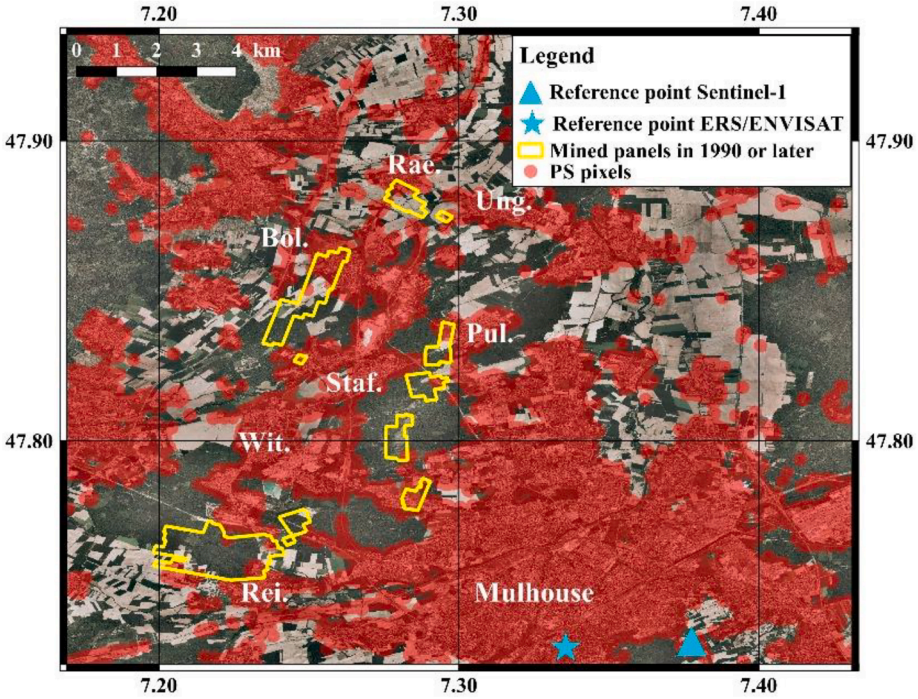

Fig. 3. Location of the Persistent Scatterers pixels. Area covers by the PS pixels from ENVISAT track 294 (with the IGN orthophotography (2002) in background).

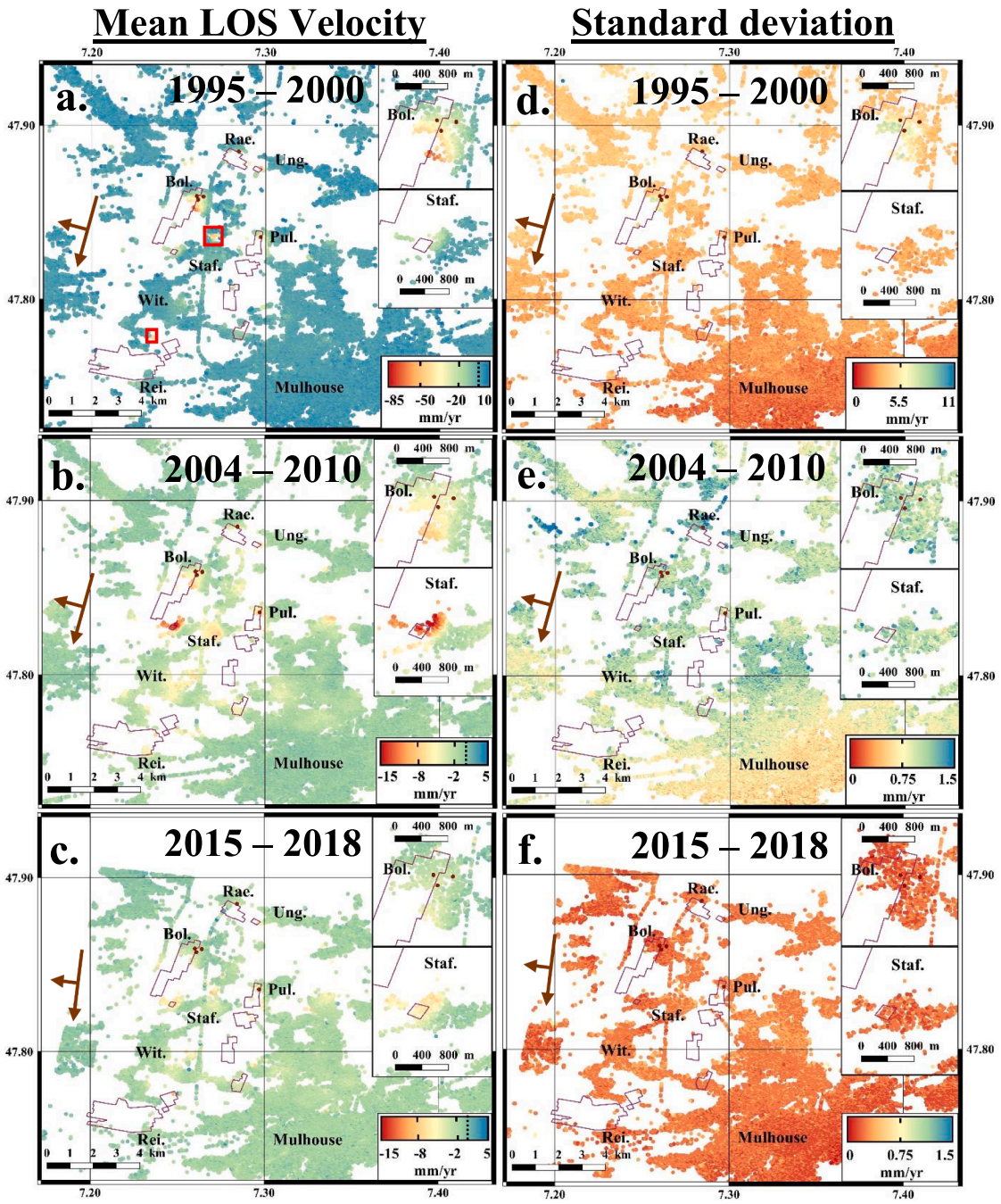

Fig. 4. Mean LOS velocity map and their associated standard deviation for a track of each satellite (a-d. ERS (track 294), b-e. ENVISAT (track 294), c-f. Sentinel-1 (track 66)). Negative LOS velocities are associated with ground displacements away from the satellite. The dotted line in the color bar indicates the value 0. Brown arrows give the azimuth and the range direction of the satellite path. Brown dots, red rectangles and purple polygons indicate the available levelling point, the location of two heaps and the extracted panels since 1990, respectively. Note that the colour scale range is different for the ERS archive. (For interpretation of the references to color in this figure legend, the reader is referred to the web version of this article.)

allows us to quantify the time evolution of the ground displacements.

4.2. Time evolution of the displacements

4.2.1. Evolution during the mining activity (1995–2000, ERS period)

In order to validate our results during the mining phase, we first compare the LOS displacement time series from the three ERS tracks. Then, we compare them to the time series of the five available levelling sites measured from February 1992 to June 2001.

As expected from the high values of the standard deviation of the mean LOS velocity, the time evolution of the LOS displacements is not linear during the whole ERS period (Fig. 5). All the time series presented in Fig. 5 show a clear decrease of the LOS velocity during the 6-year period under study (1995–2000), although the ascending time series is not well constrained during this period due to fewer images. The three InSAR datasets are in good agreement and the fit between the two descending ERS tracks validate our processing. The fit between the LOS displacement deduced from the descending tracks and the ascending track suggests that the surface motion is mainly dominated by vertical displacements. From 1999, small differences can be observed at Pulversheim (Fig. 5d) and Raedersheim (Fig. 5e). From 1995 to mid-1996, except for Pulversheim, the two descending tracks are consistent, and

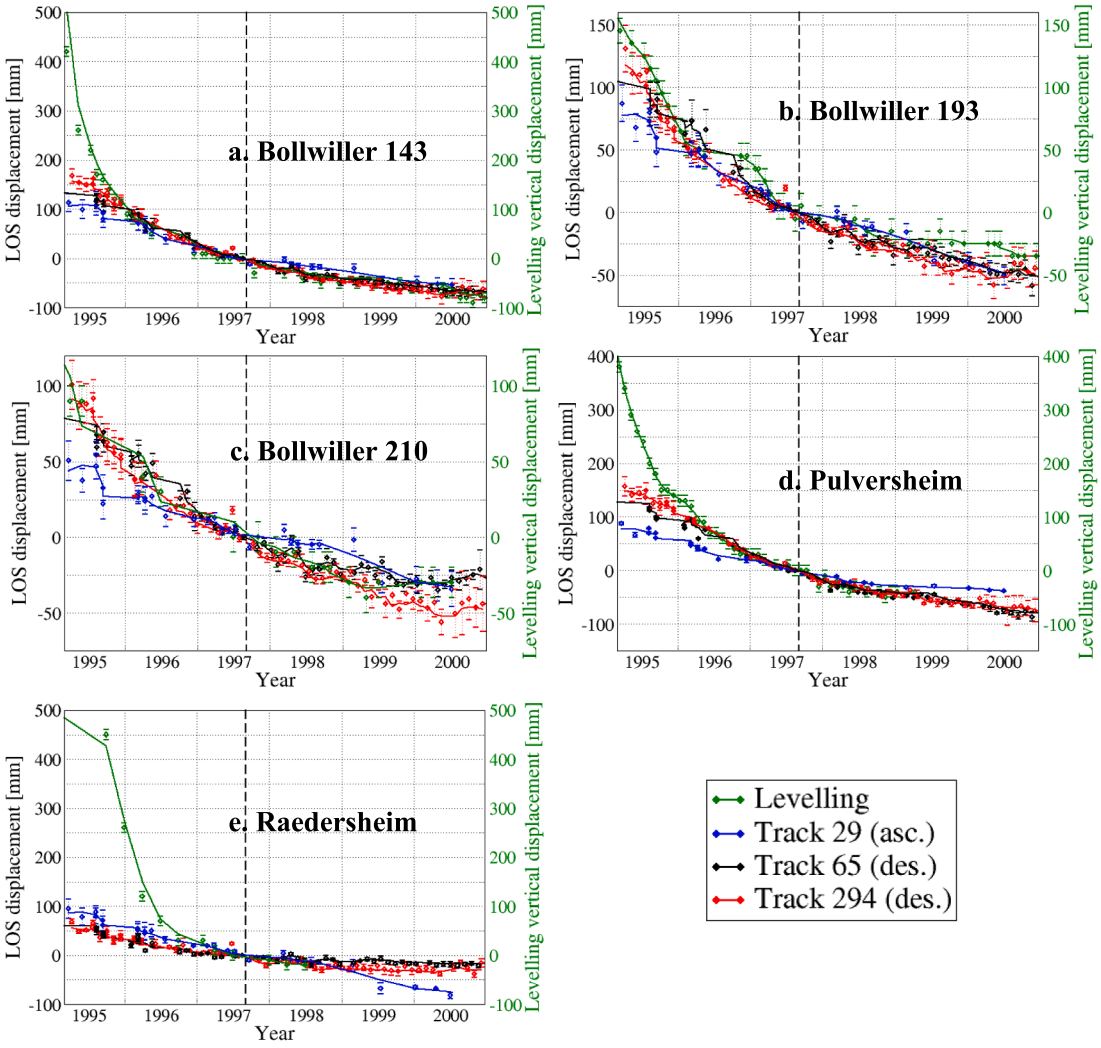

Fig. 5. Levelling and InSAR time series at the location of the five instrumented points by levelling from 1995 to 2000 (a-c. Bollwiller, d. Raedersheim., e. Pulversheim). The continuous lines show the displacements using a 2 month-long sliding window. The dotted line indicates the reference date 1997/09/03. Time series are shifted to a common zero based on the displacement difference linearly interpolated between the closest dates before and after the reference date.

show faster displacements than the InSAR results deduced from the ascending archive. This could be due to significant horizontal displacements between acquisition dates causing miscalculations during the unwrapping process. Surface subsidence is accompanied by radial horizontal surface displacements towards the centre of the subsiding area, especially during mining extraction at depth. Therefore, the difference of measurements between ascending and descending tracks could result from the horizontal displacements for the 1995–1996/1997 period. However, no horizontal displacements have been monitored by the MDPA, which prevents us from validating their amplitude over this period.

InSAR and levelling time series cannot be compared easily since none of the data are absolute. Therefore, we plot the vertical displacement levelling time series by arbitrarily setting the measurement value to 0 at the date 1997/09/03. The displacements measured by InSAR and levelling are consistent for the levelling points 193 and 210 in Bollwiller (Fig. 5b–c). However, they differ at Bollwiller 143 (Fig. 5a), Pulversheim (Fig. 5d) and Raedersheim (Fig. 5e) since only 20% to 50% of the cumulative levelling displacements are retrieved using InSAR. This discrepancy is mainly restricted in the first few months of the time series (1995–1996). From 1997, the InSAR and levelling are consistent until the date of the last levelling campaign for each location, which confirms the verticality of the detected displacements. Regarding the time series of Bollwiller 210 (Fig. 5c), small discrepancies can be observed in 1999 and 2000. Nevertheless, the observed differences remain within the error bars. Regarding the time series of the track 29 in 1999 and 2000, small discrepancies might appear due to a small number of available SAR images over this period. Areas with low pixel density can be affected by these discrepancies, such as the levelling sites of Pulversheim and Raedersheim (Fig. 5d–e).

For the period 1995–1996, the significant discrepancies between both methods cannot only be due to the difference of the measured component of the vector displacement (vertical for levelling, LOS for InSAR). Large difference between InSAR and levelling data would imply high horizontal displacements and displacements along the East-West direction would imply large differences between ascending and descending tracks that we do not observe. For instance, a displacement in the East direction would imply a positive displacement for a descending track, the pixel moving closer to the satellite, while it would imply a negative displacement for an ascending one, the pixel moving away from the satellite. These discrepancies highlight a main limitation of the InSAR, which is not suitable to measure large displacements with significant spatial gradients, which prevent reliable unwrapping. We therefore base our analysis of the surface motion using only the levelling data for the 1995–1996 period. Taking into account the possible occurrence of horizontal displacements and unwrapping errors, the

mean LOS velocity field over the ERS period helps to localize the main areas of deformation and its amplitude have to be taken with caution.

4.2.2. 24 years long InSAR time series of displacement

Over the ENVISAT and Sentinel-1 periods, the similarity of the time series deduced from ascending and descending archives allows us to assume that the surface motion corresponds primarily to vertical displacement. We therefore project the displacements amplitude along the vertical axis. Except for levelling and ERS results which are covering the same time period, both ENVISAT and Sentinel-1 datasets are disconnected from the other datasets. We connect the different datasets using a model of mining subsidence. The time evolution of mining surface subsidence can be described as an exponential function to reproduce the natural decay of the phenomenon over time (Knothe, 1957). The model temporal parameter can be estimated from the exploitation characteristics, the depth of the mining panel and the rate of advancement (Cui et al., 2001). Applied to the MDPA exploitations, the estimated time factor indicates a stop of the subsidence after 10 years. Our results show that subsidence is still occurring after more than twenty years. To model our observations more carefully, we add another exponential term to better constrain the long-term displacements (Eq. (1)):

$$D_v(t) = B_1 \times \exp(-\xi_1 \times t) + B_2 \times \exp(-\xi_2 \times t) \quad (1)$$

where D_v is the vertical displacement, B_1 and B_2 are constant, ξ_1 and ξ_2 two time factors (yr^{-1}). The physical implications of this model will be described in the discussion (5.2).

To obtain a full levelling-InSAR time series, three sets of parameters are estimated by performing three inversion using a nonlinear least-square method. The whole leveling measurements are used. The first set is estimated to connect the levelling-ERS time series to the ENVISAT time series. The second set is estimated to connect the levelling-ERS-ENVISAT time series to the Sentinel-1 time series. The last set is estimated by fitting the full levelling-ERS-ENVISAT-Sentinel-1 time series (Table 3). Only the third set of parameters is presented in Table 3 as being the one estimated from the whole time period (1992–2018). With those adjustments, we obtain the full time series presented in Fig. 6 with the modelled subsidence.

4.2.3. Residual subsidence

To characterise the residual subsidence, we need first to determine the date of its beginning at each measurement site. To do so, we look at the relative location between the measurement site and the advancement of the exploitation at depth, taking into account the angle of draw of 35° based on the expertise of the MDPA. From the angle of draw and the exploitation map, the residual subsidence has started in 1996 at Bollwiller (193 and 210) and 1997 at Bollwiller 143, Pulversheim and Raedersheim. Although the mining activity at depth ceased in 2002 for the entire basin, the end of the mining phase occurs earlier for most of the monitored points. From 1997 to 2002, the ongoing exploitation at depth in the vicinity of Bollwiller and Pulversheim (Supplementary Material 1) is too far from the monitored points to have any impact on the surface displacement at the levelling sites. On each time series, we note that the estimated beginning date of the residual phase corresponds to the date when displacements deduced from levelling measurements and InSAR results become consistent (Fig. 5a–e). This confirms that the surface displacements during the residual phase is dominated by vertical displacements.

At the end of the Sentinel-1 period, the total vertical displacements measured with InSAR over the residual phase at the levelling points are indicated in Table 4 with their respective mean vertical velocity over each period. Residual subsidence is given relatively to the total subsidence (Al Heib et al., 2005; Donnelly and Rees, 2001; Yao and Reddish, 1994) and is estimated for the Alsatian potassic basin to ~10% (MDPA internal communication). Our results are consistent with this value except for Raedersheim and Bollwiller 210 (Table 5). However, we note the variability of this ratio, suggesting that the total subsidence is not a reliable reference to quantify the residual subsidence. The ratio of the residual subsidence to the mined thickness for the five points are more consistent, with a mean value of 5.7%. Therefore, the mined thickness appears to be a more pertinent criterion to estimate the amplitude of residual subsidence.

Table 3
Estimated parameters at the five levelling points.

Levelling point	B_1 [m]	ξ_1 [yr^{-1}]	B_2 [m]	ξ_2 [yr^{-1}]
Bollwiller 143	8.87 ± 0.15	0.92 ± 0.02	0.30 ± 0.02	0.045 ± 0.002
Bollwiller 193	3.24 ± 0.06	0.88 ± 0.03	0.28 ± 0.02	0.048 ± 0.003
Bollwiller 210	1.62 ± 0.03	0.74 ± 0.02	0.29 ± 0.01	0.046 ± 0.002
Pulversheim	9.07 ± 0.14	0.95 ± 0.01	0.34 ± 0.01	0.057 ± 0.001
Raedersheim	0.55 ± 0.07	1.30 ± 0.04	0.30 ± 0.01	0.037 ± 0.001

5. Discussion

In this study, we take advantage of the existing large SAR datasets acquired by three generations of satellites to investigate the residual subsidence.

5.1. The anthropic or tectonic origins of the surface displacement

For most of our measurements, our analysis shows a great consistency between the mining activity at depth and the surface displacements. Nevertheless, as the results over the Staffelfelden area suggest, other sources, such as anthropic including heaps, water pumping and oil reservoirs, and natural with the tectonics might be at the origin of displacements.

The mine tailing has been set ups as heaps during the whole extraction period. A part of the wastes has been accumulated on heaps during the mining period while others were treated (waterproofing, greening, accelerated dissolution). In both cases, the surface level of heaps is modified, leading to high rate and localised displacements over two of them during the ERS period (Fig. 4a).

Because of the presence of rock salt in the heaps, highly salty water circulated in the ground in southern Alsace (Lucas et al., 2008) and has been pumped out by the MDPA since the 70′s. During the industrial period, the MDPA used underground water to extract the potash from the rock salt. Thus, pumping sites have been set up to mitigate groundwater pollution and to extract the potash at the surface. Although surface displacements due to water pumping have been evidenced using InSAR techniques (Fruneau et al., 2005), we do not see any clear spatial relation between the locations of the main deformed areas and the pumping sites (Fig. 7a).

In addition to the mining activity, three oil reservoirs have been exploited between 1954 and 1968 (Sittler, 1972): southwest of Reiningue, Bollwiller and Staffelfelden (Fig. 2). Whereas no atypical displacements are found at the first two sites, a high displacement rate (>8 mm/yr) is observed in Staffelfelden.

The fault network in the Rhine graben has been mapped mainly from seismic campaigns (eg., Lopes Cardozo and Behrmann, 2006). Mining induced fault reactivation is likely to occur in sedimentary basins (Sainoki and Mitri, 2014). In the Staffelfelden area, our results suggest a potential link between a fault and the surface deformation (Fig. 7a), since a minor fault with a throw of 300 m is identified. However, an oil reservoir is also located 1800 m below the area of deformation (Fig. 7b), in addition to the two potash layers extracted at a mean depth of 750 m until 1990.

Even though it remains difficult to discriminate the two origins of the deformation, anthropic or tectonic, these suggest that origins other than the mining activity have to be taken into account to explain the observed deformation at specific places such as Staffelfelden.

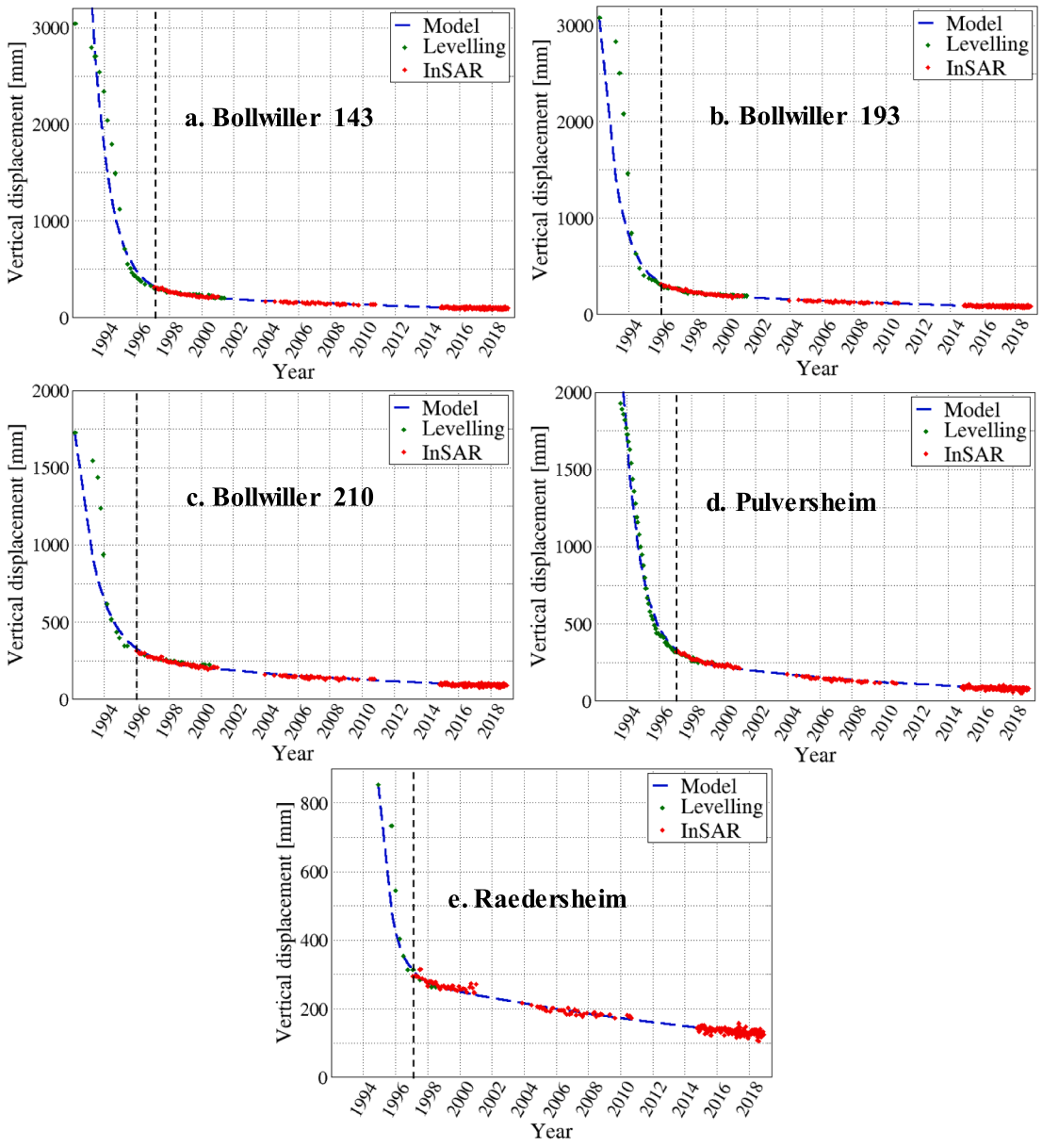

Fig. 6. Full time series at the five levelling points with the associated model from 1992 to 2018. Black dotted lines indicate the onset of the residual phase at the different levelling sites.

Table 4
Estimated vertical displacement occurring over the three monitored periods. d_v refers to the vertical displacement while v_m, to the mean vertical velocity.

Levelling point	d_v [cm] or v_m [cm/yr]	ERS (1996/1997–2000)	ENVISAT (2004–2010)	Sentinel-1 (2015–2018)	Cumulative InSAR vertical displacement [cm]
Bollwiller 143	d_v	9.4 ± 2.5	3.2 ± 1.2	1.1 ± 0.6	13.7
	v_m	2.4 ± 0.6	0.5 ± 0.1	0.3 ± 0.1	
Bollwiller 193	d_v	12.0 ± 2.5	2.9 ± 1.3	1.0 ± 0.6	15.9
	v_m	2.4 ± 0.5	0.4 ± 0.1	0.3 ± 0.1	
Bollwiller 210	d_v	10.5 ± 3.5	2.8 ± 1.4	0.9 ± 0.6	14.2
	v_m	2.1 ± 0.7	0.4 ± 0.1	0.2 ± 0.1	
Pulversheim	d_v	10.8 ± 2.4	5.8 ± 1.2	1.2 ± 0.4	17.8
	v_m	2.7 ± 0.6	0.8 ± 0.1	0.3 ± 0.1	
Raedersheim	d_v	4.7 ± 1.0	4.4 ± 1.5	1.7 ± 0.7	10.8
	v_m	1.2 ± 0.3	0.6 ± 0.1	0.4 ± 0.1	

5.2. *Mechanisms driving the residual subsidence*

Regarding longwall extractions associated with caving, mining subsidence is driven by three sources: the closure due to elastic deformation, the inelastic deformation, and the closure of both fracture and void. The caving consists in the collapse of the roof to backfill the gasps created by the extraction. The goaf refers to the area containing the collapsed materials, on a height between twice and ten times the

Table 5
Cumulative residual subsidence and its relative amplitude to the total subsidence (levelling and InSAR) and the mined thickness. The active mining subsidence is defined as the sum of the initial and the mining phase subsidence. The whole period 1996/1997 – 2018 is taken into account for the residual subsidence (InSAR) while only the period until 1995/1996 for the active mining (levelling).

Levelling point	Active mining subsidence (levelling) [cm]	Residual mining subsidence (InSAR) [cm]	Residual mining subsidence/ total subsidence [%]	Residual mining subsidence/ mined thickness [%]
Bollwiller 143	273	22	7.5	5.6
Bollwiller 193	278	24	7.9	6.2
Bollwiller 210	141	22	13.5	5.6
Pulversheim	234	25	9.7	6.3
Raedersheim	54	15	21.7	4.9

mined thickness depending on the swelling ratio. Nevertheless, the residual void volume is quite important after the caving. Further impact of the caving is the stress relaxation due to the collapse of upper materials. The stress field will evolve toward a new balance, leading to the progressive compaction of the goaf at depth (Marts et al., 2014).

To estimate the time duration of the residual subsidence, we use a sum of two exponentials. With our model, we distinguish two subsidence sources associated with a respective time factor: the first source (ξ_1) corresponds to the overburden response, and the second one (ξ_2) to the goaf compaction. In the case of a single exponential (Knothe, 1957), the time factor ξ_1 is estimated based on the rate of advance V and the depth of the exploitation H_0 (Cui et al., 2001, Eq. (2)), and is used to characterize the mechanical and physical properties of the overburden:

$$-\frac{V \times \ln(0.02)}{1.4 \times H_0} \leq \xi_1 \leq -\frac{V \times \ln(0.02)}{1.2 \times H_0} \quad (2)$$

In the case of Pulversheim (depth of 1 km, advance rate of 250 m/yr), Bollwiller (depth of 0.9 km, advance rate of 300 m/yr) and Raedersheim (depth of 0.85 km, advance rate of 450 m/yr), the factor ξ_1 ranges are [0.84 0.98], [0.78 0.91] and [1.48 1.73], respectively. Except for Raedersheim, these values ranges fit with our observations (Table 3). After ten years, this exponential term is negligible. The time factor ξ_2 is one order of magnitude lower, with value between 0.03 and 0.06 yr^{-1}, consistent with the occurrence of subsidence over decades. Thus, residual subsidence is mainly driven by the goaf compaction and this might explain the observed relation between the mined thickness and the amplitude of the residual subsidence. However, the deduction of the goaf compaction rate at depth from this simple model is not straightforward since the measured displacements at the surface is the response of the system to the void closure (Sroka et al., 2011). Hence, our second exponential term is related to many phenomena, including the void closure. The creation of a geomechanical model would lead to a proper interpretation of the monitored signals and their sources.

Eq. (2) is based on two assumptions: an angle of draw between 30 and 35°, and a residual subsidence of 2% of the total subsidence. Subsidence analysis from the MDPA confirms an angle of draw of 35°. From our results, we show that the residual subsidence is at least 4 times greater than the 2% assumed (Table 5). The case study used to validate the relationship in Cui et al. (2001) also presents a residual subsidence greater than 2% of the total subsidence. Nevertheless, the relationship satisfies the observations in both studies. Another way to formulate this second assumption would be that, at the beginning of the residual phase, 98% of the subsidence related to the overburden response has occurred.

6. Conclusion

Mining subsidence has been detected and monitored by levelling and InSAR over a 24-year period. Displacements occur at a large rate and are localized during the mining period. With a lower amplitude, the mining subsidence remains significative over decades after the end of the underneath exploitation, which corresponds to the residual phase. As the monitoring of surface displacement is required by authorities during the

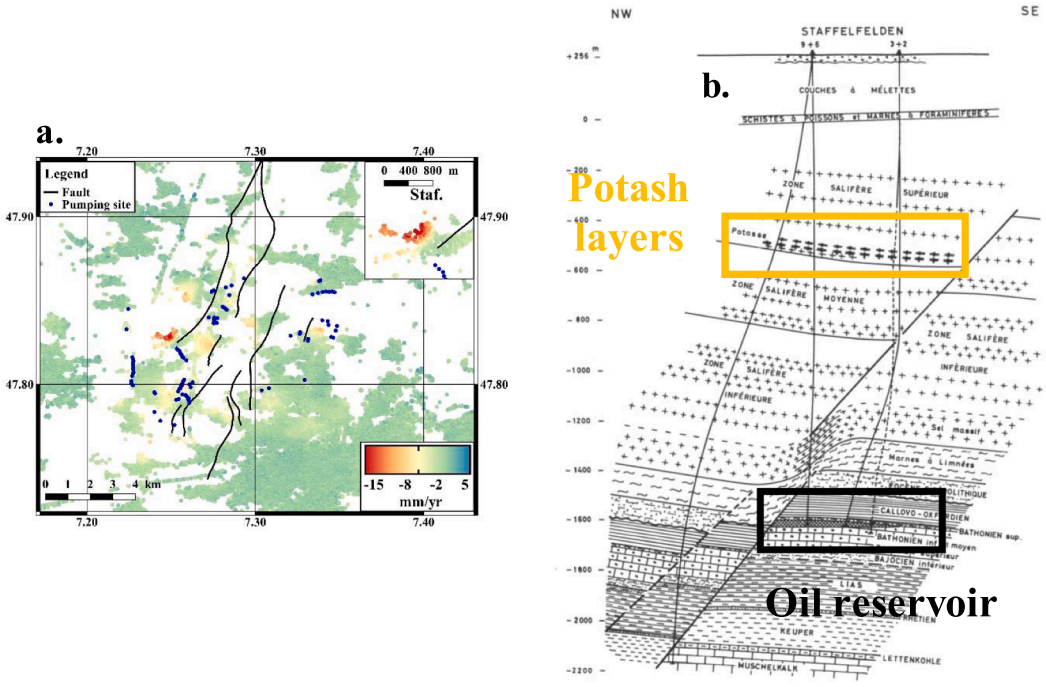

Fig. 7. Potential sources of surface displacements. a: Mean LOS velocity during ENVISAT period with the pumping sites (blue circles) and faults (black lines); b. Geological section across Staffelfelden (adapted from Sittler, 1972). The location of faults at depth has been projected at the surface. (For interpretation of the references to color in this figure legend, the reader is referred to the web version of this article.)

mining operation, our results suggest that this monitoring should be conducted as well beyond the mining operation to assess the related hazard and the risk in urbanized region. As shown with the levelling measurements, the mining phase cannot be correctly recovered using only the available InSAR dataset covering the 90's period due to both the temporal sparsity of the SAR image acquisitions and the high amplitude of the surface displacements. Our results help to better characterize the time evolution of the surface subsidence during the residual phase and the parameters controlling its amplitude over several time scales. We show that the mined thickness of the mining panel is one of the main controlling parameters. Our InSAR results also evidenced atypical residual subsidence, such as in the town of Staffelfelden, probably related to the combination of the mining activity at depth, the exploitation of an oil reservoir and/or tectonics in this region affected by regular low and moderate seismicity and crustal deformation (Henrion et al., 2020).

From the levelling measurements and our InSAR results, we propose a model to estimate the characteristic time periods of the sources driving the mining subsidence. The first time factor represents the inelastic response of the overburden. The second time factor, mainly constrained by our InSAR results, appears to be related to the void closure. These results presented in this study represent an important dataset to constrain geomechanical modelling in order to quantify the closure rate at depth. Such modelling could be crucial to estimate the time evolution of the void closure in mining panels where the accessibility is impossible or reduced.

CRediT authorship contribution statement

Guillaume Modeste: Writing - original draft, Software, Validation, Formal analysis, Investigation, Data curation, Visualization. **Cécile Doubre:** Conceptualization, Writing - review & editing, Supervision, Resources, Project administration. **Frédéric Masson:** Conceptualization, Writing - review & editing, Supervision, Resources, Project administration, Funding acquisition.

Declaration of Competing Interest

The authors declare the following financial interests/personal relationships which may be considered as potential competing interests: This study is financially supported by the MDPA.

Acknowledgements

The authors are grateful to the MDPA and DREAL for their encouraging support and their trust, and François H. Cornet for his discussions. The authors are grateful to the anonymous reviewers for their constructive comments on the manuscript. SAR images have been provided by ESA. The study is financially supported by the MDPA.

Appendix A. Supplementary material

Supplementary data to this article can be found online at https://doi.org/10.1016/j.jag.2021.102392.

References

Al Heib, M., Nicolas, M., Noirel, J.F., Wojtkowiak, F., 2005. Residual subsidence analysis after the end of coalmine work. Example from Lorraine colliery, France. <ineris-00972515>. In: Symposium Post Mining, p. 2005 10..

Amelung, F., Galloway, D.L., Bell, J.W., Zebker, H.A., Laczniak, R.J., 1999. Sensing the ups and downs of Las Vegas: InSAR reveals structural control of land subsidence and aquifer-system deformation. Geology 27, 483–486. https://doi.org/10.1130/0091-7613(1999)027<0483:STUADO>2.3.CO;2.

Berardino, P., Fornaro, G., Lanari, R., Sansosti, E., 2002. A new algorithm for surface deformation monitoring based on small baseline differential SAR interferograms. IEEE Trans. Geosci. Remote Sens. 40, 2375–2383. https://doi.org/10.1109/TGRS.2002.803792.

Blanc-Valleron, M.-M., 1991. Les formations paléogènes évaporitiques du Bassin Potassique de Mulhouse et des bassins plus septentrionaux d'Alsace. PhD thesis., Document du BRGM. Éd. du BRGM, Orléans.

Cendon, D., Ayora, C., Pueyo, J., Taberner, C., Blancvalleron, M., 2008. The chemical and hydrological evolution of the Mulhouse potash basin (France): are "marine" ancient evaporites always representative of synchronous seawater chemistry? Chem. Geol. 252, 109–124. https://doi.org/10.1016/j.chemgeo.2008.01.019.

Chrzanowski, A., Monahan, C., Roulston, B., Szostak-Chrzanowski, A., 1997. Integrated monitoring and modelling of ground subsidence in potash mines. Int. J. Rock Mech. Min. Sci. 34, 55.e1–55.e16. https://doi.org/10.1016/S1365-1609(97)00229-3.

Colesanti, C., Mouelic, S.L., Bennani, M., Raucoules, D., Carnec, C., Ferretti, A., 2005. Detection of mining related ground instabilities using the Permanent Scatterers technique—a case study in the east of France. Int. J. Remote Sens. 26, 201–207. https://doi.org/10.1080/0143116042000274069.

Cui, X., Wang, J., Liu, Y., 2001. Prediction of progressive surface subsidence above longwall coal mining using a time function. Int. J. Rock Mech. Min. Sci. 38, 1057–1063. https://doi.org/10.1016/S1365-1609(01)00061-2.

Declercq, P.-Y., Walstra, J., Gérard, P., Pirard, E., Perissin, D., Meyvis, B., Devleeschouwer, X., 2017. A study of ground movements in brussels (Belgium) monitored by persistent scatterer interferometry over a 25-year period. Geosciences 7, 115. https://doi.org/10.3390/geosciences7040115.

Donnelly, L.J., Rees, J.G., 2001. Tectonic and mining induced fault reactivation around Barlaston on the Midlands Microcraton, North Staffordshire, UK. Q. J. Eng. Geol. Hydrogeol. 34, 195–214. https://doi.org/10.1144/qjegh.34.2.195.

Farr, T.G., Kobrick, M., 2000. Shuttle radar topography mission produces a wealth of data. Eos Trans. Am. Geophys. Union 81, 583. https://doi.org/10.1029/EO081i048p00583.

Foumelis, M., Blasco, J.M.D., Yves-Louis Desnos, Engdahl, M., Fernández, D., Veci, L., Lu, J., Wong, C., 2018. ESA SNAP – StaMPS Integrated Processing for Sentinel-1 Persistent Scatterer Interferometry. https://doi.org/10.13140/rg.2.2.25803.90405.

Fruneau, B., Deffontaines, B., Rudant, J.-P., Le Parmentier, A.-M., 2005. Monitoring vertical deformation due to water pumping in the city of Paris (France) with differential interferometry. C.R. Geosci. 337, 1173–1183. https://doi.org/10.1016/j.crte.2005.05.014.

Fuhrmann, T., 2016. Surface Displacements from Fusion of Geodetic Measurement Techniques Applied to the Upper Rhine Graben Area. https://doi.org/10.5445/IR/1000056073.

Guéguen, Y., Deffontaines, B., Fruneau, B., Al Heib, M., de Michele, M., Raucoules, D., Guise, Y., Planchenault, J., 2009. Monitoring residual mining subsidence of Nord/Pas-de-Calais coal basin from differential and Persistent Scatterer Interferometry (Northern France). J. Appl. Geophys. 69, 24–34. https://doi.org/10.1016/j.jappgeo.2009.02.008.

Hanssen, R.F., 2010. Radar Interferometry: Data Interpretation and Error Analysis, Remote Sensing and Digital Image Processing. Kluwer Academic Publishers, Dordrecht.

Henrion, E., Masson, F., Doubre, C., Ulrich, P., Meghraoui, M., 2020. Present-day deformation in the Upper Rhine Graben from GNSS data. Geophys. J. Int. 223, 599–611. https://doi.org/10.1093/gji/ggaa320.

Hooper, A., Bekaert, D., Spaans, K., Arıkan, M., 2012. Recent advances in SAR interferometry time series analysis for measuring crustal deformation. Tectonophysics 514–517, 1–13. https://doi.org/10.1016/j.tecto.2011.10.013.

Hooper, A., Segall, P., Zebker, H., 2007. Persistent scatterer interferometric synthetic aperture radar for crustal deformation analysis, with application to Volcán Alcedo, Galápagos. J. Geophys. Res. 112 https://doi.org/10.1029/2006JB004763.

Hooper, A., Zebker, H.A., 2007. Phase unwrapping in three dimensions with application to InSAR time series. J. Opt. Soc. Am. A: 24, 2737. https://doi.org/10.1364/JOSAA.24.002737.

Knothe, S., 1957. Observations of surface movements under influence of mining and their theoretical interpretation. In: Proceedings of the European Congress on Ground Movement. Presented at the Proceedings of the European Congress on Ground Movement, pp. 210–218.

Kratzsch, H., 1983. Mining Subsidence Engineering. Springer Berlin Heidelberg, Berlin, Heidelberg. https://doi.org/10.1007/978-3-642-81923-0.

Lopes Cardozo, G.G.O., Behrmann, J.H., 2006. Kinematic analysis of the Upper Rhine Graben boundary fault system. J. Struct. Geol. 28, 1028–1039. https://doi.org/10.1016/j.jsg.2006.03.010.

Lucas, Y., Haushalter, M., Clement, A., Fritz, B., Chabaux, F., 2008. Hydrogeochemical Modelling of the Alsace Groundwater Pollution by the Potash Mine Spoil Heaps. In: Post-Mining Conference. Presented at the Post-Mining Conference, Nancy, France.

Marts, J., Gilmore, R., Brune, J., Bogin Jr, G., Grubb, J., Saki, S., 2014. Dynamic gob response and reservoir properties for active longwall coal mines. Min. Eng. 66, 59–66.

Massonnet, D., Feigl, K.L., 1998. Radar interferometry and its application to changes in the Earth's surface. Rev. Geophys. 36, 441–500. https://doi.org/10.1029/97RG03139.

Oppliger, G., Coolbaugh, M., Shevenell, L., 2006. Improved visualization of satellite radar InSAR observed structural controls at producing geothermal fields using modeled horizontal surface displacements. GRC Trans. 30, 927–930.

Raymond, D., Rudant, J.-P., 1997. ERS-SAR interferometry: Potential and limits for mining subsidence detection. European Space Agency-Publications-ESA SP 414, pp. 541–544.

Sainoki, A., Mitri, H.S., 2014. Dynamic behaviour of mining-induced fault slip. Int. J. Rock Mech. Min. Sci. 66, 19–29. https://doi.org/10.1016/j.ijrmms.2013.12.003.

Samsonov, S., d'Oreye, N., Smets, B., 2013. Ground deformation associated with post-mining activity at the French-German border revealed by novel InSAR time series

method. Int. J. Appl. Earth Obs. Geoinf. 23, 142–154. https://doi.org/10.1016/j.jag.2012.12.008.

Shanker, P., Casu, F., Zebker, H.A., Lanari, R., 2011. Comparison of persistent scatterers and small baseline time-series InSAR results: a case study of the San Francisco Bay area. IEEE Geosci. Remote Sens. Lett. 8, 592–596. https://doi.org/10.1109/LGRS.2010.2095829.

Sittler, C., 1972. Le pétrole dans le département du Haut-Rhin. Bilan d'un siècle et demi de recherches et d'exploitations. Sci. Géol. Bull. 25, 151–161. https://doi.org/10.3406/sgeol.1972.1412.

Sroka, A., Tajdus, K., Preusse, A., 2011. Calculation of subsidence for room and pillar and longwall panels. In: 11th Underground Coal Operators' Conference. Presented at the 11th Underground Coal Operators' Conference, University of Wollongong, pp. 83–90.

Whittaker, B.N., Reddish, D.J., 1989. Subsidence: Occurrence, Prediction, and Control. Elsevier Amsterdam.

Yao, X.L., Reddish, D.J., 1994. Analysis of residual subsidence movements in the UK coalfields. Q. J. Eng. Geol. Hydrogeol. 27, 15–23. https://doi.org/10.1144/GSL.QJEGH.1994.027.P1.04.